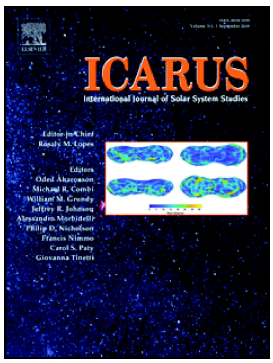

OSSOS. XVII. An upper limit on the number of distant planetary objects in the Solar System

Edward Ashton, Brett Gladman, J.J. Kavelaars, R. Lynne Jones, K. Simon Krughoff, Mike Alexandersen, Michele T. Bannister, Ying-Tung Chen, Stephen Gwyn, Jean-Marc Petit, Kathryn Volk

PII: S0019-1035(20)30177-9

DOI: https://doi.org/10.1016/j.icarus.2020.113793

Reference: YICAR 113793

To appear in: *Icarus*

Received date: 30 June 2018

Revised date: 25 February 2020

Accepted date: 14 March 2020

Please cite this article as: E. Ashton, B. Gladman, J.J. Kavelaars, et al., OSSOS. XVII. An upper limit on the number of distant planetary objects in the Solar System, *Icarus* (2020), https://doi.org/10.1016/j.icarus.2020.113793

OSSOS. XVII. An upper limit on the number of distant planetary objects in the Solar System

Edward Ashton[a], Brett Gladman[a], J. J. Kavelaars[b], R. Lynne Jones[c], K. Simon Krughoff[d], Mike Alexandersen[e], Michele T. Bannister[f], Ying-Tung Chen[e], Stephen Gwyn[b], Jean-Marc Petit[g] and Kathryn Volk[h]

[a]*Dept. of Physics and Astronomy, University of British Columbia, 6244 Agricultural Road, Vancouver, BC, V6T 1Z1, Canada*
[b]*Herzberg Astronomy and Astrophysics Research Centre, National Research Council of Canada, 5071 West Saanich Rd., Victoria, BC V9E 2E7, Canada*
[c]*Astronomy Department, University of Washington, Box 351580, Seattle, WA 98195-1580, USA*
[d]*LSST Project Office, 950 N Cherry, Tucson AZ 85719, USA*
[e]*Institute of Astronomy and Astrophysics, Academia Sinica; 11F of AS/NTU Astronomy-Mathematics Building, Nr. 1 Roosevelt Rd., Sec. 4, Taipei 10617, Taiwan*
[f]*Astrophysics Research Centre, School of Mathematics and Physics, Queen's University Belfast, Belfast BT7 1NN, United Kingdom*
[g]*Institut UTINAM UMR6213, CNRS, Univ. Bourgogne Franche-Comté, OSU Theta F-25000 Besançon, France*
[h]*Lunar and Planetary Laboratory, The University of Arizona, 1629 E University Blvd, Tucson, AZ 85721*

✉ eashton@phas.ubc.ca (E. Ashton)
ORCID(s): 0000-0003-4143-8589 (M. Alexandersen);
0000-0003-3257-4490 (M.T. Bannister); 0000-0001-7244-6069 (Y. Chen);
0000-0001-8736-236X (K. Volk)

Abstract
Beyond the giant planets there is a collection of bodies left over from the epoch of planet formation. The objects that are just beyond Neptune are more easily detected than those that journey hundreds of au away; all such highly eccentric objects have been observed inside 150 au. We are interested here in a population of Pluto to Mars-sized planets that were almost certainly present in the early Solar System, some of which may now be stranded in the distant Solar System. Using data from the Outer Solar System Origins Survey (OSSOS), which covers ~ 167 square degrees down to r ~ 25, we searched for objects beyond 300 au using a rarely used search technique. To find such objects we created catalogues of all the sources that were stationary (to the level of the astronomical seeing) in three images taken over 2 hours. We then searched for which such 'stationary' objects were not present days/weeks/months before and after. Although other

astronomical phenomena (e.g. supernovae) were discovered, no slow moving Solar System object was found. From the null detection and using a survey simulator, we obtain a model-dependent 95 % upper limit of ~ 1000 on the number of 'planetary' objects (with absolute magnitudes, H_r, less than 2) in the distant Solar System. To our knowledge this is the first published limit for objects of this scale beyond 300 au. We show that if there are a small number of Mars-scale objects still in the distant Solar System, despite being brighter they may have escaped detection in other surveys due to their slow rates of motion.

Highlights

- We searched ~ 167 square degrees for distant (>300 au) Solar System objects down to $m_r = 25.5$.
- Using a survey simulator we turned our null result into an upper limit of $\sim$ 1000 Pluto sized objects in the distant Solar System.
- Our analysis highlights interesting aspects in the distribution of detection distances, at both perihelion and aphelion.

Keywords: Kuiper belt; Planetary Formation; Dwarf planets

1. Introduction

Planet formation is a complex process. Regardless of the details of how planets form, there are planets and minor bodies of all sizes observed or inferred in both the Solar System and other stellar systems. The planet building process (and subsequent collisional erosion) yields the current size distribution.

Trans-Neptunian Objects (TNOs) are icy bodies out beyond Neptune. The very upper end of the TNO size distribution is not well determined due to small number statistics; there are currently only three known Pluto-sized objects (Pluto, Eris, and captured Triton).

There were likely at least 1000 Pluto scale objects produced during planet formation in the outer Solar System [23, 14]. Even though almost all of these Pluto-sized minor bodies were ejected from the Solar System, it would be very surprising if the three already discovered Pluto-sized TNOs in the Solar System were all that remained. If there was another Pluto-sized or larger object in the Solar System, where would it be? If the object was within 165 au it had a roughly $2/3$ chance of being found by the Schwamb et al. [18] (or the smaller/shallower surveys of Sheppard et al. [22], Rabinowitz et al. [17], Bannister [1] and Brown et al. [6]) search of the ecliptic, unless it was particularly highly inclined, or currently in front of the galactic plane. This leaves the region beyond 165 au as the most likely to yield new detections. The majority of TNO surveys are unable to detect objects moving < 0.5"/hr, which corresponds to 300 au at opposition. We were thus motivated to search existing multi-night survey data looking for objects beyond these distances.

At the beginning of this 2017 investigation, the two surveys that could detect Pluto-sized or larger objects beyond 300 au distance were the Spacewatch Survey [12], which covered a sky area of $\sim$ 8,000 square degrees, and aforementioned Schwamb et al. [18] survey, which covered $\sim$ 12,000 square degrees. Larsen et al. [12] estimate they were able to detect the motions of objects out to 1250 au although, as they stated, with their magnitude limit of $m_r \sim 20.5$ they can only detect Jovian sized objects at this distance. Schwamb et al. [18] indicate that they were able to

detect the motions of objects out to 1000 au, although their limiting magnitude of m_r = 21.3 corresponds to Pluto only out to 165 au. After our current work began, two more surveys have been used to search for slowly moving objects. The Pan-STARRS data has been searched for objects out to 2000 au [9]. The survey has a limiting magnitude of m_r = 22.5, which would detect Pluto out to 250 au, and covered nearly the whole sky north of -30^o in declination (excluding the galactic plane). Sheppard and Trujillo [21] searched a thousand square degrees and state sensitivity to objects out to 500 au; because multiple telescopes were used, their limiting m_r magnitude varied from 24 to 25.5, with a majority of their observations having depths $m_r \approx$ 24-24.6.

Figure 1 shows the combinations of distance and object size that can be detected in the three of the surveys described above and in this work. In regards to detecting Pluto sized objects at distances greater than 300au, the surveys of Schwamb et al. [18] and Holman et al. [9] are not deep enough. Sheppard and Trujillo [21], on the other hand, would have been able to see Pluto sized objects out to almost 500 au, but only with a small fraction of their survey. Most of their survey could not see objects fainter than m_r = 24.6, which is Pluto at 350 au.

Figure 1: Minimum visible planet radius as a function of distance for four surveys: Schwamb et al. [18] (blue), Holman et al. [9] (magenta), Sheppard and Trujillo [21] (red), and this work (black). The solid lines represent the limit of the region of phase space which an object can be detected by the surveys. The diagonal lines correspond to the limiting R band magnitude, these values are converted to radius by scaling Pluto's apparent magnitude (using Pluto's albedo). The shaded green area is the region of phase space that this work is sensitive to, with light green if there is overlap with other surveys, and dark green being parameter space unique to this study.

In this paper we present the data set used (Section 2), details of our searching method and the results (Section 3), and how we turned the null result into an upper limit on the number of Pluto sized objects in the outer Solar System (Section 4).

2. Data

The data used for this work come from the Outer Solar System Origins Survey (OSSOS), designed to detect and track a large sample of TNOs in the 10-300 au distance range. The survey covers a small fraction of the the ecliptic's area: $\sim$ 167 square degrees that is split up into eight, roughly equally sized, regions of sky known as blocks [3]. OSSOS' depth depends on the image quality (IQ) of the triplets (see next paragraph).Thus the limiting magnitude varies from block to block and ranges from m_r = 24.5 to 25.2.

The OSSOS observing cadence can be conceptually broken up into two parts, the imaging for discovery on one night ('triplets') and images for tracking, and thus orbit determination, taken on various other nights ('confirmation'). The triplet consists of three 287-sec images taken with 1-hour spacing, which were used to discover the TNOs using a moving-object detection software pipeline [15]. The confirmation images are single images taken at a variety of time intervals both before and after the triplet. The majority of the confirmation images reach deeper depths than the triplet images, either via a better IQ, longer exposure time, or a wider filter [3]. Most fields had a

least one confirmation image taken in the a couple of days after the triplet, at least one a week after, at least one at $\pm$ one month, and one at $\pm$ two months. In some cases there were confirmation iamges that were $\pm$ three months from the triple. This cadence produced complete TNO orbital linkages; here we use the confirmation images for a different purpose (see below). The OSSOS cadence also contains confirmation images taken in the following opposition, these confirmation images were only used in this work if a block was considered to contain too few confirmations in the discovery opposition. For a more complete understanding of OSSOS please refer to Bannister et al. [2] and Bannister et al. [3]

3. Method

Because we expect only a few Pluto-sized objects to be in the outer Solar System today and OSSOS only covered a small fraction of the ecliptic, we did not expect to find any objects in this search. Thus the goal of this work was to do a quick search to estimate a first upper limit on the number of distant Pluto-sized objects in the Solar System, to a factor of two to three accuracy. Thus, when in our data analysis we realised that it was possible to do something 'slightly better' but at a much larger time expense, we chose to mildly sacrifice precision.

To detect TNOs, OSSOS employed the commonly used method of searching for linearly moving objects in three short-cadence discovery triplet images. A TNO's on-sky rate of motion at opposition, in "/hour, can be approximated by $150/d$, where d is the object's heliocentric distance in au. The original search set a lower limit of ~ 0.5"/hour, which would comfortably detect motion in the triplet images. Motion slower than 0.5"/hour corresponds to objects beyond 300 au but resulted [2] in a rapidly increasing number of false positives due to stationary sources being flagged as moving due to centroiding jitters. OSSOS thus did not search these rates. In order to detect these (< 0.5"/hour) Slow Moving Objects (SMOs) we use a different technique, searching for objects that appeared stationary in the triplet images, within some tolerance, but did not reappear in most of the confirmation images (some similarities to [6]). This allows us to be sensitive to Pluto-scale and larger objects at great distance.

The first step of our algorithm is to create a catalogue of all the objects that appear stationary in each triplet. This was achieved by matching sources in the existing OSSOS source catalogues. Each triplet image has two source catalogues, one created using wavelets [15] and the other using S-Extractor [5]. For an object to be classed as 'stationary' it needed to appear in all six catalogues of the triplets (2 catalogue creation methods for each of the 3 images). When matching sources from two different catalogues, the tolerance used was a weighted combination of the seeing on the two images and the distance an object moving at 0.5"/hour would have traveled. The seeing was used as a proxy for the uncertainty in the source position since the catalogues did not contain an estimate for these uncertainties.

We then identify all of the confirmation images where the (RA, Dec) sky position of a given stationary object is on the pixels of that confirmation image. This task was not trivial due to the slow drift in image position that OSSOS used to minimise TNO loss off the edges of the imaged sky areas. This necessitated a highly accurate absolute plate solution, which OSSOS already had. Each confirmation image that contained the desired (RA,Dec) is considered 'on-pixels' for a particular stationary object. The catalogues for each on-pixels confirmation images are searched for a match to the stationary object. The seeing of the worst triplet image and the confirmation image, added in quadrature, were used as the tolerance for this search. If the stationary object was matched to a source in the on-pixels confirmation image catalogue, then the

object was considered 'found' on that confirmation image. Each stationary object thus has a different number of potential detections on the full set of confirmation images.

Some of the confirmation images had poorer IQ than the triplet and thus the faintest stationary objects were not detected on all of its on-pixels confirmation images. Therefore we needed to classify the stationary objects as either being bright, where the object should always be detected regardless of the seeing, or faint, where the object was below the mag limit on some fraction of the worst confirmation images. This boundary between the bright and faint was determined by simply examining graphs showing at which flux there was a drop off in average number of confirmation detections per stationary object (i.e. the average number of detections per stationary object is fairly constant for fluxes brighter than this boundary and steadily decreases as the flux decreases below it). For the OSSOS fields and depths, the ratio of faint to bright objects was approximately unity. We determined that this drop off simply starts when the object is too faint to be seen on the worst confirmation image, at which point the likelihood of finding these faint objects again in the confirmation image depends on a comfirmation image's seeing. If a faint stationary object was not found on a confirmation image whose (RA,Dec) is present, but that confirmation image's seeing was bad enough to fail a quality check, then that confirmation image is not counted as on-pixels for the stationary object. We assume that the bright objects should always be detected in the confirmation images, independent of the seeing. On average there were about 10 useful confirmation images per stationary object.

Any stationary object that did not reappear in any of the confirmation images, which would be the desired signal of a real SMO, were placed in a candidate list. To negate the possibility of a SMO not making it into the candidate list due to a chance cosmic ray or asteroid causing a false detection at that position on a confirmation image, stationary objects that were found on up to two confirmation images were included in the candidate list. The remaining objects had multiple detections and were considered 'confirmed' stationary objects.

All candidates were vetted by an operator looking at cutouts of the images centred on the candidate. In a rapid first pass, only the triplet images were visually examined to reject anything that was obviously not a point source. In a second pass, all of the images where a candidate is on-pixels were looked at (the triplet, and all confirmation images where that (RA,Dec) is available).

After applying this method to each field of each OSSOS block, no SMOs were found. The number of first pass candidates per square degree ranged from tens to a few hundred, *with roughly a third of these candidates making it to the second pass*. Almost all of the candidates were false positives, the exception being 66 detected supernovae (see Fig 2 for an example). These supernovae were at peak brightness near the time of the triplet, so they usually were not seen in the confirmation images before the triplet and only visible in a couple of the confirmation images taken a few days/weeks after. *Thus not exceeding the maximum two detection over all confirmation images needed to still be a candidate.*

Figure 2: *Images of a supernova event (centre of the red circles) in the outskirts of a distant galaxy that was identified as a SMO candidate by our code, because it was only detected by the code on two (out of 24) confirmation images. The top row contains images taken 2 months (left) and 1 month (right) before the triplet. The three triplet images are in the middle row. The bottom row contains images taken a day (left), 1 month (middle) and 8 months (right) after the triplet. The sudden appearance and fading out on the timescale of a month is characteristic of a type 1a supernova. Each cut out is about 10" wide.*

The vast majority of false positives suggested for vetting were very faint stars or caused by halos of bright stars. That is, in the diffraction halo of bright stars local peaks in brightness can occur and the pipeline identifies these as (stationary) objects, or a faint source in a very good-seeing triple may be not get into the confirmation catalogs. In both these cases the nature of the candidate is obvious to the human operator. A rarer and interesting type of false positive are optical ghosts caused by internal reflections of very bright stars which then appear as faint sources with normal (or nearly normal) point-spread functions. The barely different pointings for each triple image caused the location of the optical ghost to move, but only barely perceptibly and thus less than the stationary tolerance for the triplets. For the confirmation images, however, the blocks shifted enough that the optical ghost is no longer anywhere near its position in the triplets. This mimics the signal that of a real SMO with the main difference being the usually non-linear movement of the optical ghosts in the triple. For the few cases where the non-linearity was less pronounced, we examined the projected position of the optical ghost in the confirmation images a few days later. Because the optical ghost had apparent rates of only a few tenths of an arcsecond per hour, their projected positions a day later were less than 10 arcseconds away from their triplet positions. If they were actually SMOs finding them in the confirmation image a couple of days later would have been trivial. None of the 'optical ghosts' re-appeared, thus proving that these signals were not SMOs. Over the entire survey, 26 optical ghosts were found.

4. Survey Simulator

Even though no SMOs were discovered, we can use this null result, along with the fact that the initial OSSOS search did not find any nearby objects of this size, to place an upper limit on the number of large (Pluto-sized and bigger) TNOs in the outer Solar System, subject to some assumptions. Firstly we assume that the code would have found a real SMO, if there was one above the mag limits, since objects that behaved similarly to a SMO (optical ghosts) made it into the candidate list. Therefore no planting and finding of artificial objects was required to establish a magnitude detection limit, because we assume that the efficiency of the code to find a real SMO of a certain r-band magnitude is the same as that established for an OSSOS TNO in that same block [3], allowing us to use the OSSOS survey simulator, both of which rely on the detection efficiency of the triplet, as the recovery/confirmation rate is very high. This is an approximation, but good enough for our factor of 2 to 3 estimate.

The OSSOS survey simulator works by creating one object at a time from an input orbital and size distribution model and assessing whether this object would have been found by OSSOS. For more detail see Kavelaars et al. [11], Lawler et al. [13].

The orbital distribution we use for potential large semi-major axis objects consists of a uniform semi-major axis, a, ranging from 150 au to 999 au. We assume that the pericentre distance, q, distribution is uniformly distributed starting from q = 37 au out to 99 au. The inclination distribution used is the typical sin i times a Gaussian; because a SMO would be either a scattering or detached object and thus will be part of the hot population, we use a width of 13° [16]. All the other parameters (longitude of ascending node, the argument of perihelion, and the mean anomaly) are uniformly distributed from 0 to 360°.

For the simulated size distribution, we wanted to examine objects ranging from the smallest object that we would have been able to detect up to a Mars-sized object. A Mars-sized object (with Pluto's albedo) would have an absolute magnitude, H_r, of -3. *Known large TNO's*

have comparatively high albedos; if distant large TNOs objects were to have lower albedos then they would have to be larger in size for us to detect them (the product of albedo and reflecting area being constant). The smallest object that we can detect would have an apparent mag of 25.5 at 300 au, corresponding to an object with $H_r \approx 0.7$. The matching tolerance used in making the stationary catalogue allowed the algorithm to find objects moving slightly faster than 0.5"/hour, due to the seeing of the triples. The closest object the algorithm deployed here could detect was actually slightly closer than 300 au. Due to this, and that the range would be a convenient 5 magnitudes, we decided to simulate objects down to $H_r = 2$ (a range spanning 5 magnitudes corresponds to a change in radius by a factor of 10). Therefore the H_r mag range we used was -3 to 2.

For the functional form of the absolute magnitude distribution of our simulated population, we look to known TNOs whose distribution is often represented with an exponential law of the form

$$N(<H) \propto 10^{\alpha H} \tag{1}$$

where N($< H$) is the cumulative number of objects that have an absolute magnitude of 'H' or less and α is the logarithmic slope. The value of α is known to differ for different H ranges. For objects brighter than H_v of 6, the known TNOs exhibit two slopes with a transition at $H_v \sim 3$ (Figure 3). The values for α are $\alpha = 0.14$ for the shallow slope and $\alpha = 0.61$ for the steep slope. The largest H_r value in our desired range, $H_r = 2$, corresponds to $H_v \sim 2.5$, which is lower than the apparent transition near 3. Thus the simulated sample is situated in the range where the H_r distribution slope is shallow. Because there is no clear argument that the slope would change for TNOs larger than Pluto, we used a logarithmic size distribution with a slope of $\alpha = 0.14$ for the entire simulated population.

Figure 3: The cumulative heliocentric absolute visual magnitude H_v distribution of the known TNOs down to $H_v = 8$ (blue line). Two exponential functions are plotted (dashed lines) to guide the eye and match the slope of the data; note that these are not fits to the data. The logarithmic slope, α, of each exponential function is displayed above each line. The obvious roll-over beyond $H_v \sim 6$ is due to the increasing observational incompleteness of fainter TNOs. Data obtained from the Minor Planet Center.

To get a 95 % upper limit from the survey simulator we need to estimate the population size needed so that the chance of getting no detections is < 5 %. This corresponds to having an expected value of 3 simulated detections (for Poisson statistics, as $e^{-3} \simeq 5$ %). Therefore we ran the survey simulator until we got 3 detections, and the number of objects generated serves as an estimate of the 95% upper limit on the true intrinsic population of these large objects. We ran the simulator to get 1000 independent estimates for this upper limit (only the random seed changed). A histogram of the 1000 trials is shown in Figure 4. The sample has a median value of 1100. Although this value is model dependent, as stated earlier we were only looking for a factor of two

to three accuracy, and we found that moderate changes in the parameters did not affect our conclusions.

Figure 4: A histogram constructed from the 1000 estimates of the 95% confidence upper limt on the population of large ($-3 < H_r < 2$) planetary scale bodies currently in the outer Solar System. The median of this distribution (dashed line) is taken to be our best estimate for the upper limit.

While studying the survey simulation, we noted an interesting aspect of the observational biases. To study the distance distribution of detectable objects, we define a quantity *F*, which we refer to as the fractional orbital distance, to measure how far beyond perihelion the objects were when detected.

$$F = \frac{d - q}{Q - q} \tag{2}$$

where *d* is the object's heliocentric distance at detection, and *q* and *Q* are the objects perihelion and aphelion distance, respectively. Thus *F* moves smoothly from 0 to 1 as *d* goes from *q* to *Q*, and its distribution provides insight into the concentration of detection at perihelion or aphelion. Unsurprisingly, the *intrinsic* distance distribution for these highly eccentric objects (black line, left panel in Figure 5) has a peak at $F = 1$ due to a long residence near aphelion caused by Kepler's second law. The small spike at perihelion (F=0) is due objects having close to zero radial motion and thus spend more time near the circle $r = q$ (see Figure 6), even without detection bias. We then compare the *F* distribution of the simulated detections for 3 different magnitude ranges ($-3 < H_r < -2$, $-1 < H_r < 0$, $1 < H_r < 2$). The smallest object range (dwarf planets) are predominantly found at low *F* values (near perihelion) due to the fact that a vast majority of them are only above the magnitude limits when near perihelion. This phenomenon, that perihelion flux bias wipes out the aphelion spike in the distance distribution, is not new and was first illustrated in Jones et al. [10]. In contrast the left panel in Figure 5 shows that the largest detected objects are more uniformly spread in detection *d* (example Gerdes et al. [7]) and in addition still maintain a strong detection spike at aphelion. This is simply because the Mars-scale objects can be detected further out, including the frequent case of being near aphelion. The implication is that past surveys with similar depths could have detected the flux from a Mars-sized object; at this size the most likely single case is being above the magnitude limit while near apocentre. *Even though such an object would be visible*, at hundreds of au away it was almost certainly below the survey rate cuts and would not be identified as a moving target *and thus missed. However, most of the previous wide-field surveys searching for distant Solar System objects do not go to 24th magnitude, but should still be able detect (in terms of flux) a Mars-sized object out to few hundred au. According to Schwamb et al. [20] & Schwamb et al. [19] the current pipeline for detecting moving objects in Large Synoptic Survey Telescope (LSST) cannot detect the motion of objects beyond 200 au. Unless LSST include a search method, like ours, that examines multi-night data for objects that do not move perceptibly in a single night, they could miss a Mars-sized object near apocentre.*

Figure 5: The fraction of objects with a certain fractional orbital distance, F (left), and the true amonaly (right) for different H_r magnitude ranges are red for -3 $< H_r <$ -2, green for -1 $< H_r <$ 0 and magenta for 1 $< H_r <$ 2. Each group has around 90,000 values which are split up into 15 bins. The intrinsic population (black line) is added for reference. The spike of the intrinsic population near F=0 is real and due the radial component of the heliocentric velocity being small. Note that a range of semi-major axes are represented here, allowing for a few of the even physically smallest (magenta-coded) objects to be detected near apocentre.

The fractional orbital distance is related to the true anomaly of course, but provides different insights. The right panel in Figure 5 shows the true anomaly distribution for both the intrinsic population and for the simulated detections for the same three H_r-magnitude ranges as the left panel; we only plot the true anomaly from 0 to π since it is symmetric around π. The intrinsic distribution nicely shows how this large-*e* population spend more time at higher true anomaly due to Kepler's Second Law. It also shows how the detection bias eventually truncates the distribution at large-enough true anomaly, producing a detection maxima in the range of true anomaly 2 - 2.5 (for these relatively large objects). These maxima correspond to the small bumps in the F distributions between $F = 0.1 - 0.4$ in the left panel of Figure 5. What the true anomaly plot hides is the increase in detections near perihelion, which is represented as the spikes at $F = 0$ in the left hand plot, which is present even in the intrinsic distribution but is magnified in the detected sample. This occurs because while the time spent near a true anomaly of zero is indeed small, the time spent near $r \sim q$ is not (Figure 6). This perihelion spike (which is even more pronounced for lower eccentricity orbits) is an important phenomenon in flux-limited surveys if one is going to determine whether the distribution of detection distances matches a model because large swaths of true anomaly have nearly the same reflected flux, and it is the distance distribution that is thus critical. Gladman et al. [8] clarifies how this is also affected by, and can thus help constrain, the absolute magnitude distribution.

Figure 6: Schematic of an eccentric orbit (solid ellipse) that has been divided into segments of equal true anomaly. Dotted circles represent the perihelion and aphelion distances. Near perihelion, an object's heliocentric distance is relatively constant over a large range of true anomalies, producing a concentration of detections with $r \sim q$ (as demonstrated in Figure5)

5. Discussion & Conclusion

After searching through the $\sim$ 167 square degrees of the OSSOS data for a slow moving object beyond 300 au, 66 supernovae and 26 optical ghosts were found but no slow-moving solar system objects. By simulating high semi-major axis TNOs we obtain an understanding of the statistics of the objects we were sensitive to. Although this work is the first search sensitive to Mars-scale objects at 500-1000 au, the upper limit of $\sim$ 1000 objects from -3 $< H_r <$ 2 is not

very constraining. Half of this distribution ($H_r <$ -0.5) corresponds to Pluto-scale and larger objects. Estimates based on the fact that three such objects (Pluto, Eris and Triton) are currently known have been used to predict that $\sim$ 1000 - 4000 must have existed in the very early Solar System during the planet migration phase (e.g. Nesvorný and Vokrouhlický [14]), given an estimated 'retention efficiency' of order 10^{-3}. Thus, a current upper limit of 1000 such bodies is not very constraining to these late-stage planetary formation models, as those models would indicate <10 such objects likely remain in the outer reaches of the Solar System. Our modeling does indicate, however, that if a few such objects still exist in the scattering or detached populations of the outer Solar System, they may very well have been near aphelion moving so slowly that previous deep ($m_R \sim 24$–25) surveys would have been unable to detect them. *LSST would need to alter their pipeline to be able to detect these extremely slow moving targets using their multi-night data.* If we crudely scale from our 0.3% of detection to LSST, by saying that survey will cover 50 times the ecliptic sky area of OSSOS down to a similar depth, LSST has a 15% chance of finding a single (-3 $< H_r <$ 2) 'planet', if these objects are distributed in the scattering population roughly like as assumed here. *Because the H-magnitude distribution is shallow, usage of large apertures is not as important as sky coverage; the sum of existing wide-field surveys (eg. Sheppard and Trujillo [21], Bernardinelli et al. [4]), some of which is far from the ecliptic, provides an even smaller chance of success than LSST of finding such a distant planet.*

6. Acknowledgements

This work was supported by funding from the National Sciences and Engineering Research Council of Canada.

References

[1] Bannister, M.T. , 2014 . Bright Trans-Neptunian Objects in the Southern Sky . Ph.D. thesis. RSAA, the Australian National University.. Canberra .

[2] Bannister, M.T. , et al., 2016 . The Outer Solar System Origins Survey. I. Design and First-quarter Discoveries . The Astronomical Journal 152 , 70 . arXiv:1511.02895 .

[3] Bannister, M.T. , et al., 2018 . OSSOS. VII. 800+ Trans-Neptunian Objects—The Complete Data Release . The Astrophysical Journal 236 , 18 . doi: 10.3847/1538-4365/aab77a , arXiv:1805.11740 .

[4] Bernardinelli, P.H. , et al., 2019 . Trans-Neptunian objects found in the first four years of the Dark Energy Survey . arXiv e-prints , arXiv:1909.01478 arXiv:1909.01478 .

[5] Bertin, E. , Arnouts, S. , 1996 . SExtractor: Software for source extraction. Astronomy and Astrophysics Supplement 117 , 393–404 .

[6] Brown, M.E. , et al., 2015 . A Serendipitous All Sky Survey for Bright Objects in the Outer Solar System . The Astronomical Journal 149 , 69 . doi: 10.1088/0004-6256/149/2/69 , arXiv:1501.00941 .

[7] Gerdes, D.W. , et al., 2017 . Discovery and Physical Characterization of a Large Scattered Disk Object at 92 au . The Astrophysical Journal 839 , L15 . doi: 10.3847/2041-8213/aa64d8 , arXiv:1702.00731 .

[8] Gladman, B. , et al., 2012 . The Resonant Trans-Neptunian Populations . The Astropnomical Journal 144 , 23 . doi: 10.1088/0004-6256/144/1/23 , arXiv:1205.7065 .

[9] Holman, M.J. , et al., 2016 . Primary results from the Pan-STARRS-1 Outer Solar System Key Project , in: AAS/Division for Planetary Sciences Meeting Abstracts #48 , p. 120.02 .

[10] Jones, R.L. , et al., 2006 . The CFEPS Kuiper Belt Survey: Strategy and presurvey results . Icarus 185 , 508–522 . arXiv:astro-ph/0510826 .

[11] Kavelaars, J.J. , et al., 2009 . The Canada-France Ecliptic Plane Survey L3 Data Release: The Orbital Structure of the Kuiper Belt . The Astronomical Journal 137 , 4917–4935 .

[12] Larsen, J.A. , et al., 2007 . The Search for Distant Objects in the Solar System Using Spacewatch . The Astronomical Journal 133 , 1247–1270 .

[13] Lawler, S.M. , et al., 2018 . OSSOS: X. How to use a Survey Simulator: Statistical Testing of Dynamical Models Against the Real Kuiper Belt . Frontiers in Astronomy and Space Sciences 5 , 14 . arXiv:1802.00460 .

[14] Nesvorný, D. , Vokrouhlický, D. , 2016 . Neptune's Orbital Migration Was Grainy, Not Smooth . The Astrophysical Journal 825 , 94 . arXiv:1602.06988 .

[15] Petit, J.M. , et al., 2004 . A highly automated moving object detection package .

Monthly Notices of the Royal Astronomical Society 347 , 471–480 . doi: 10.1111/j.1365-2966.2004.07217.x .

[16] Petit, J.M. , et al., 2017 . The Canada-France Ecliptic Plane Survey (CFEPS) High-latitude Component . The Astronomical Journal 153 , 236 . arXiv:1608.02873 .

[17] Rabinowitz, D. , et al., 2012 . The La Silla-QUEST Kuiper Belt Survey . The Astronomical Journal 144 , 140 . doi: 10.1088/0004-6256/144/5/140 , arXiv:1205.5214.

[18] Schwamb, M.E. , Brown, M.E. , Rabinowitz, D.L. , 2009 . A Search for Distant Solar System Bodies in the Region of Sedna . The Astropysical Journal 694 , L45–L48 . arXiv:0901.4173 .

[19] Schwamb, M.E. , et al., 2018 . Large synoptic survey telescope solar system science roadmap . arXiv:1802.01783 .

[20] Schwamb, M.E. , et al., 2019 . A software roadmap for solar system science with the large synoptic survey telescope . Research Notes of the AAS 3 , 51 . URL: https://doi.org/10.3847

[21] Sheppard, S.S. , Trujillo, C. , 2016 . New Extreme Trans-Neptunian Objects: Toward a Super-Earth in the Outer Solar System . The Astronomical Journal 152 , 221 . arXiv:1608.08772 .

[22] Sheppard, S.S. , et al., 2011 . A Southern Sky and Galactic Plane Survey for Bright Kuiper Belt Objects . The Astronomical Journal 142 , 98 . doi: 10.1088/0004-6256/142/4/98 , arXiv:1107.5309 .

[23] Stern, S.A. , 1991 . On the number of planets in the outer solar system - Evidence of a substantial population of 1000-km bodies . Icarus 90 .

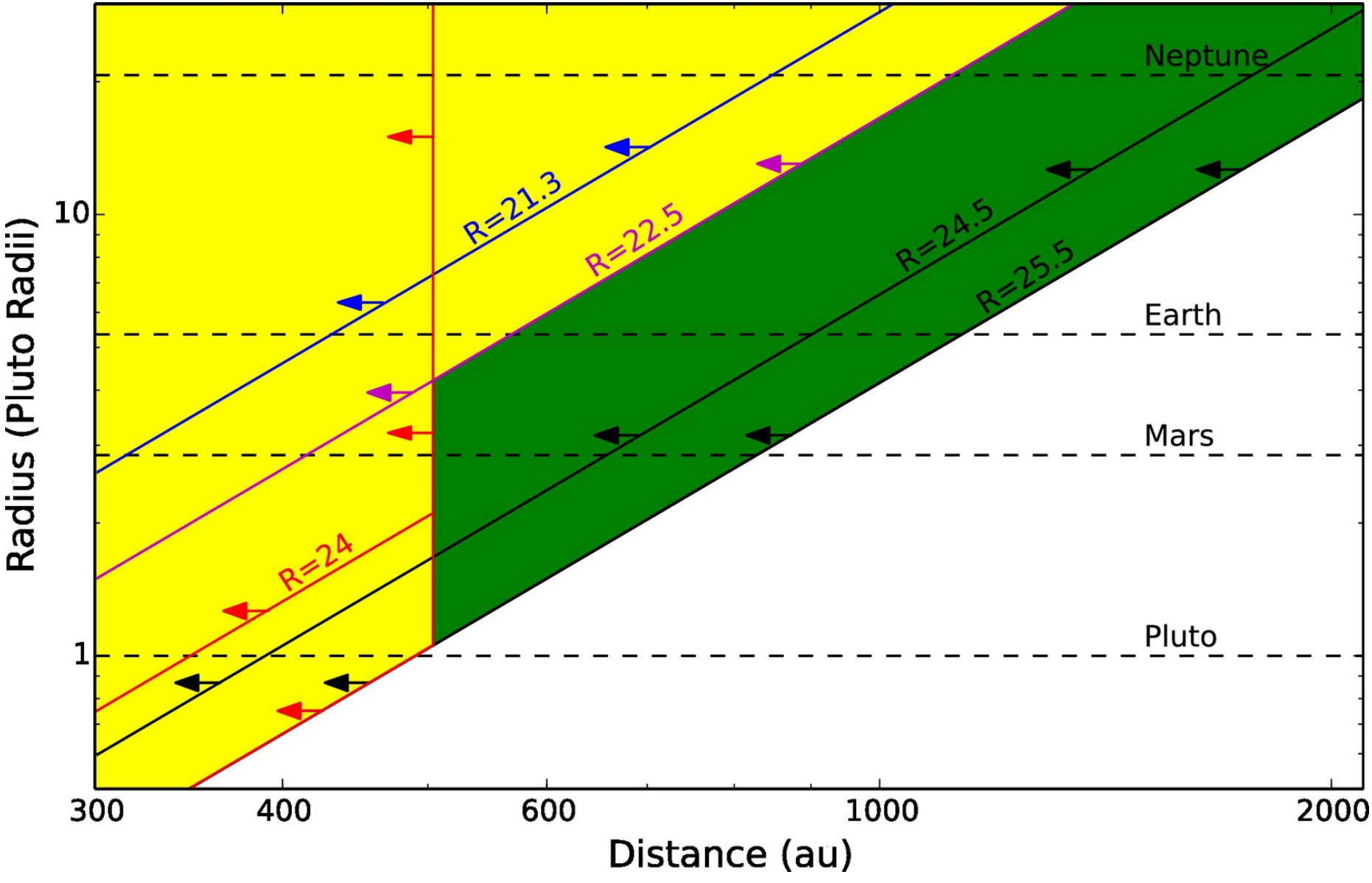
Neptune
Earth
Mars
Pluto
10
1
R=21.3
R=22.5
R=24.5
R=25.5
R=24
Radius (Pluto Radii)
300
400
600
1000
2000
Distance (au)

Figure 1

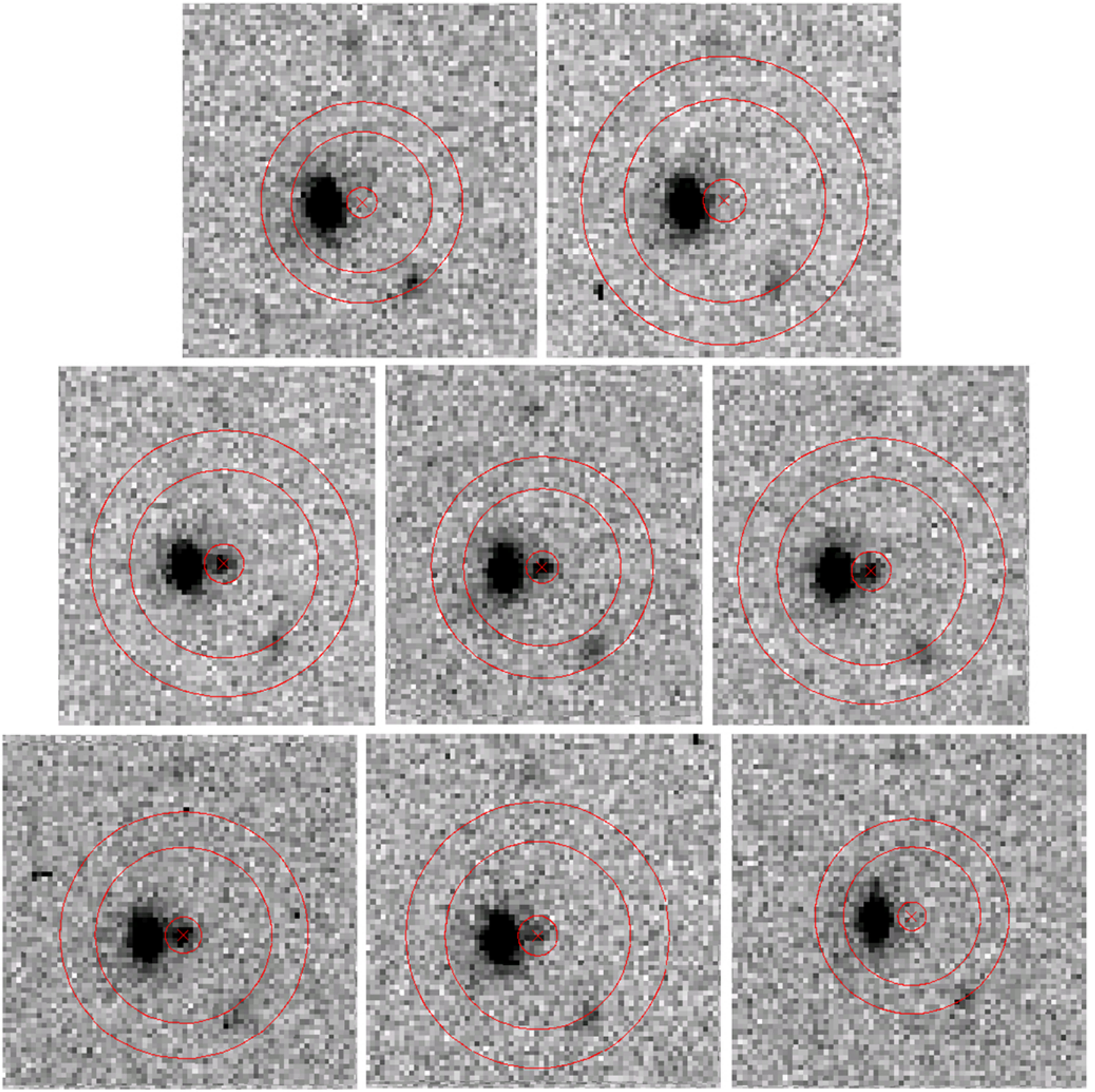

Figure 2

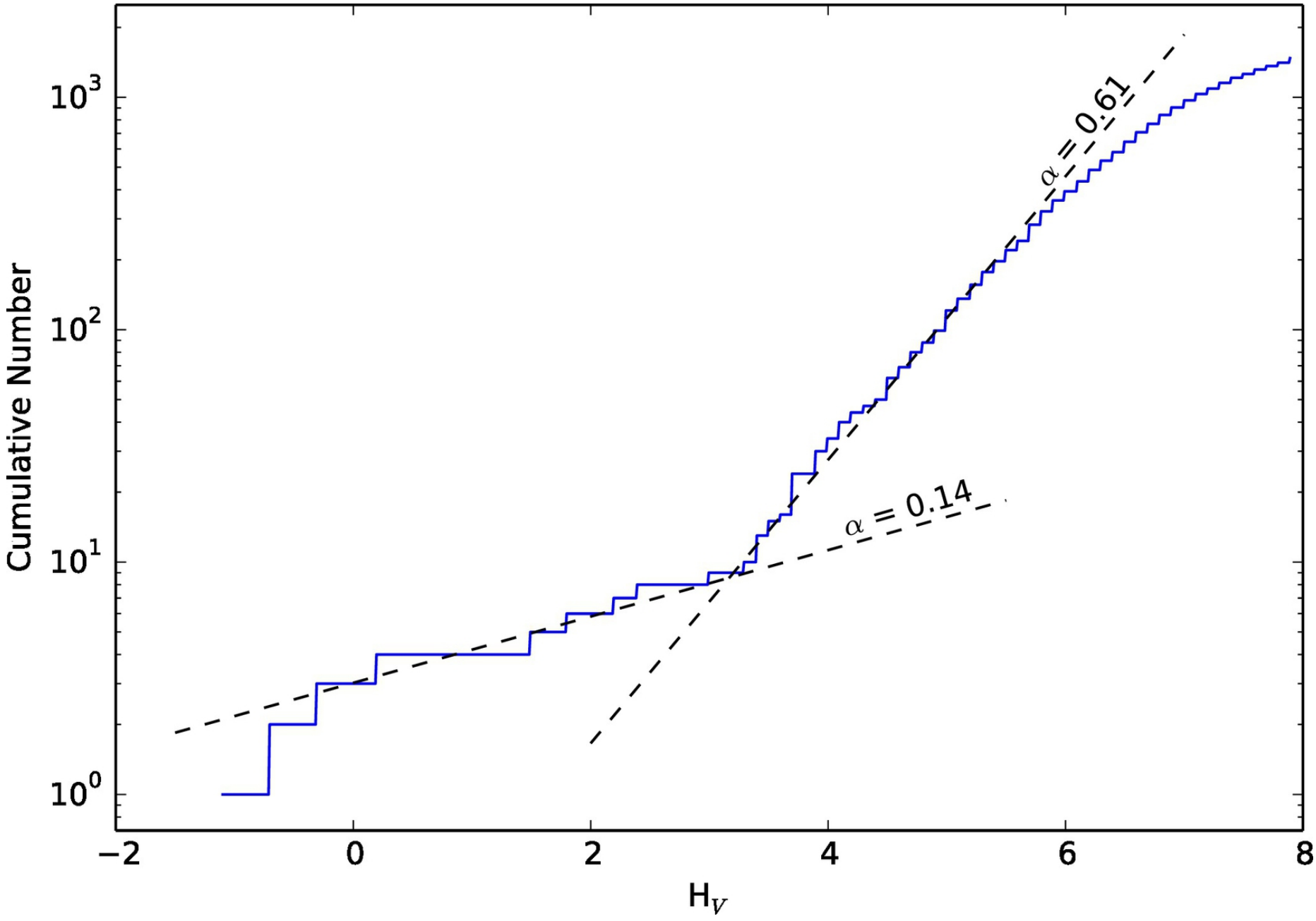
Cumulative Number
10^3
10^2
10^1
10^0
−2
0
2
4
6
8
H_V
$\alpha = 0.61$
$\alpha = 0.14$

Figure 3

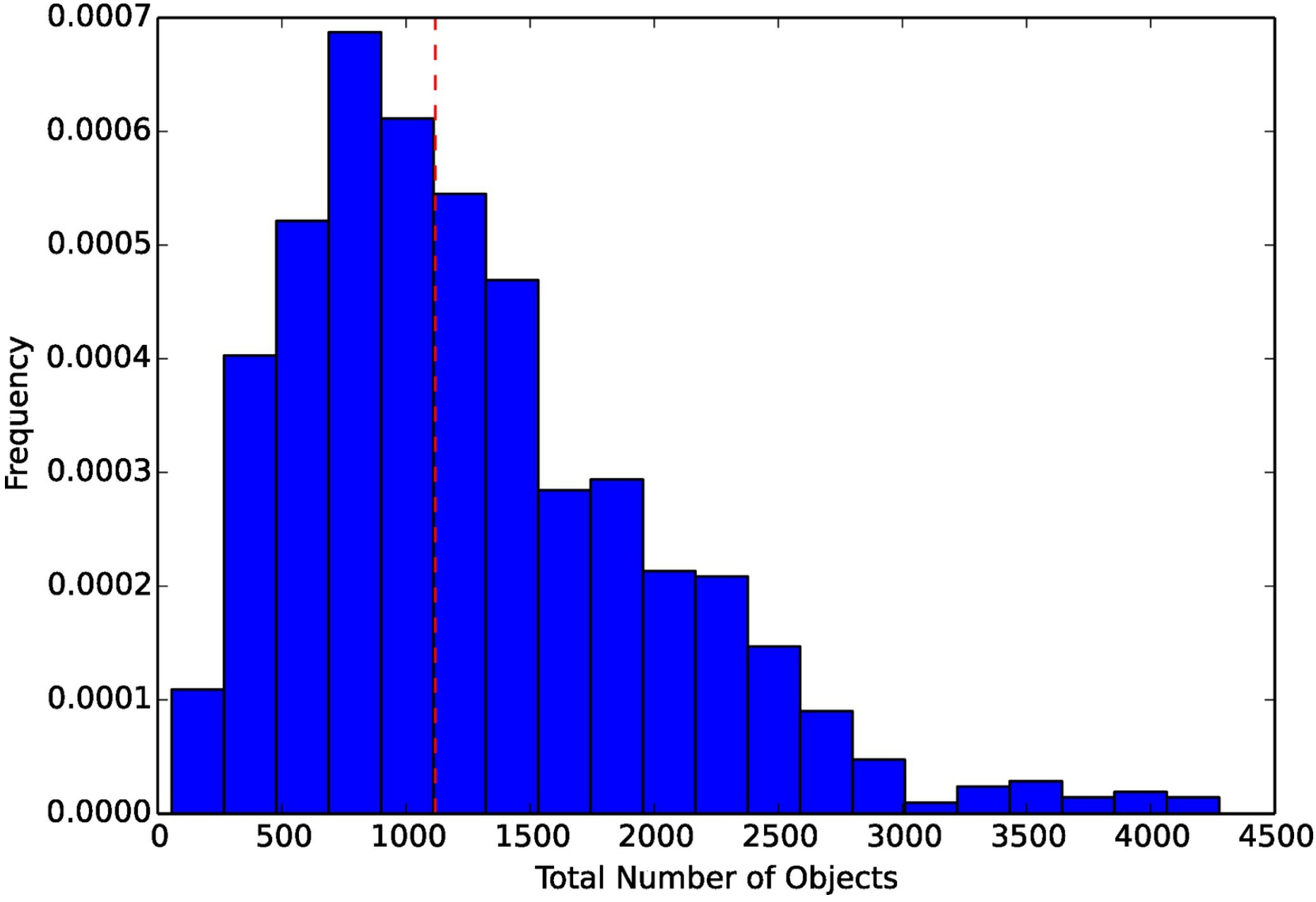
0.0007
0.0006
0.0005
0.0004
0.0003
0.0002
0.0001
0.0000
Frequency
0
500
1000
1500
2000
2500
3000
3500
4000
4500
Total Number of Objects

Figure 4

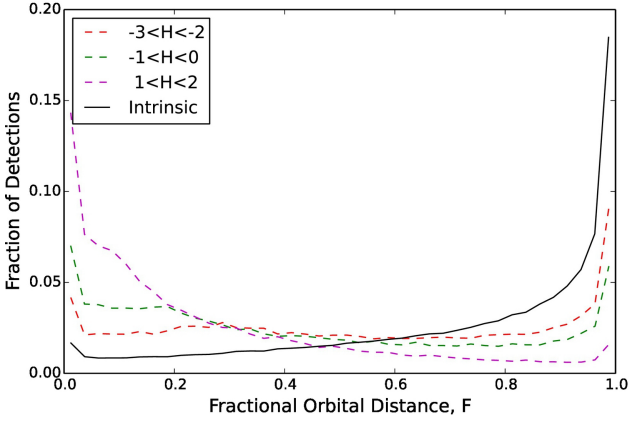
-3<H<-2
-1<H<0
1<H<2
Intrinsic
Fraction of Detections
Fractional Orbital Distance, F
0.00
0.05
0.10
0.15
0.20
0.0
0.2
0.4
0.6
0.8
1.0

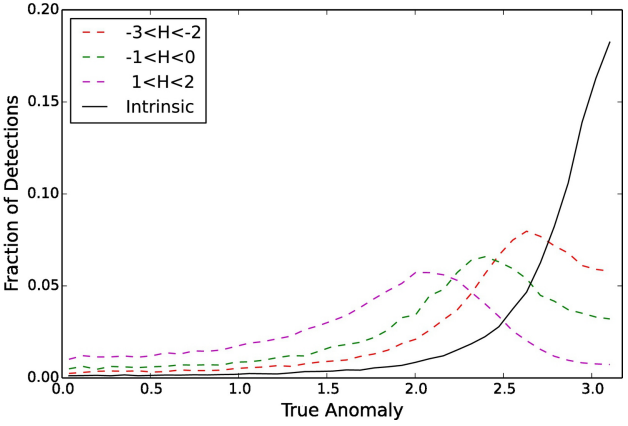
-3<H<-2
-1<H<0
1<H<2
Intrinsic
Fraction of Detections
True Anomaly
0.00
0.05
0.10
0.15
0.20
0.0
0.5
1.0
1.5
2.0
2.5
3.0

Figure 5

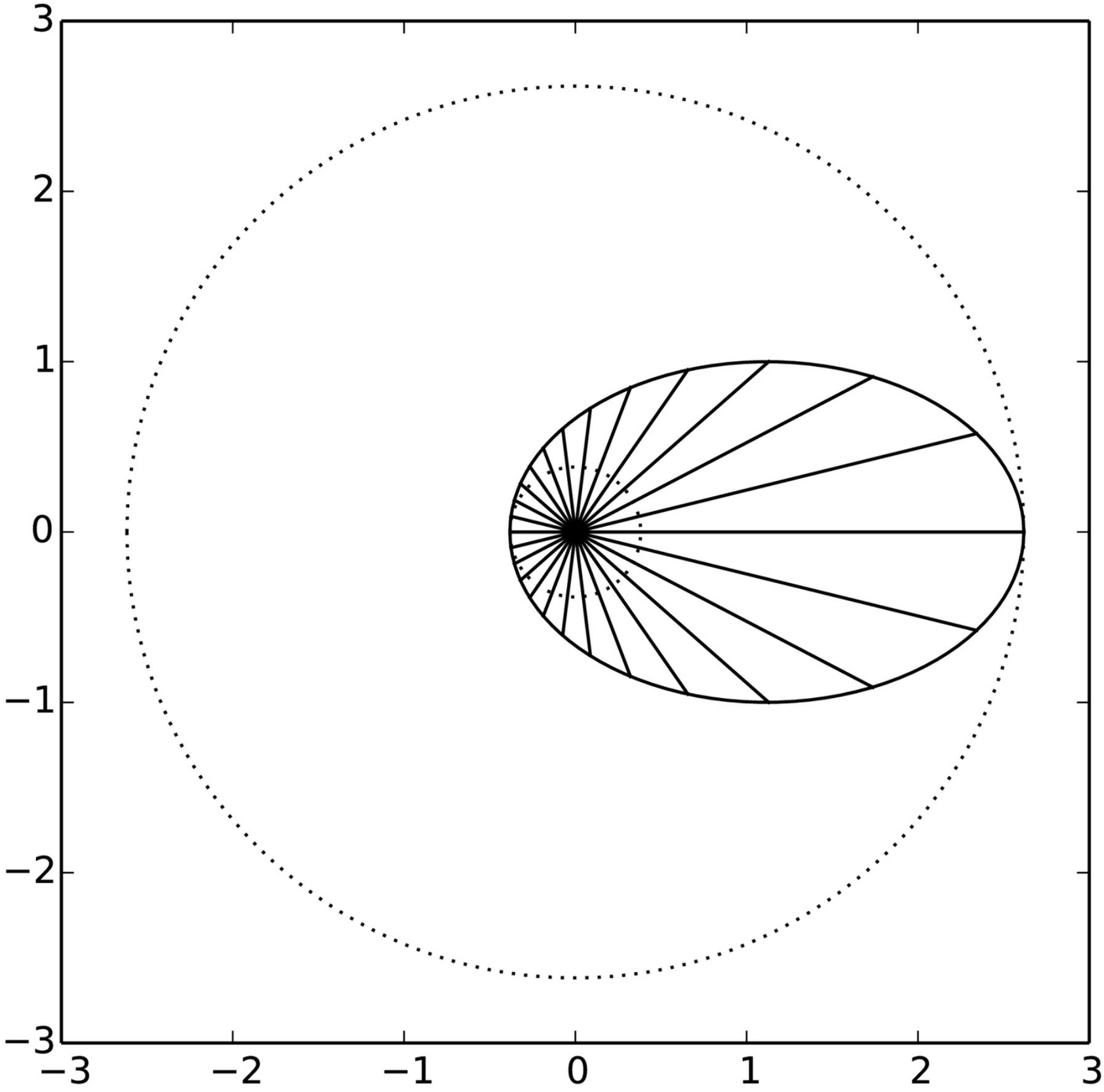

Figure 6